International Journal of Multiphase Flow 131 (2020) 103297

Contents lists available at ScienceDirect

International Journal of Multiphase Flow

journal homepage: www.elsevier.com/locate/ijmulflow

Associating void fraction signals with bubble clusters features in co-current, upward gas-liquid flow of a non-Newtonian liquid

Petros K. Gkotsis, Sotiris P. Evgenidis, Thodoris D. Karapantsios*

Department of Chemical Technology and Industrial Chemistry Faculty of Chemistry, Aristotle University, University Box 116, 541 24 Thessaloniki, Greece

ARTICLE INFO

Article history:
Received 24 January 2020
Revised 25 March 2020
Accepted 2 April 2020
Available online 23 June 2020

Keywords:
Bubble clusters
Non-newtonian liquids
Void fraction
Electrical impedance technique
Optical technique

ABSTRACT

This study investigates the behaviour of bubble clusters rising amongst single bubbles in a non-Newtonian liquid, employing: a) an ultra-sensitive electrical impedance spectroscopy technique for obtaining void fraction time-series and b) an optical method for estimating cluster size and shape. Bubble clusters cause intense void fraction signal peaks. The novelty concerns the association of signal characteristics with bubble cluster features. Therefore, useful insight on bubble clustering encountered in ultrasound medical applications (such as dissolution of blood clots during thrombosis or cancer drug delivery) is provided. Experiments are performed in co-current, upward bubbly flow. Results show a strong dependence of cluster features on gas superficial velocity (U_{sg}). Void fraction signal analysis demonstrates that peaks become sharper when bubble clusters get larger. On the other hand, time length of signal peaks remains almost constant despite the increase of cluster sizes. Additionally, bubble clusters frequency increases with U_{sg} and decreases with surfactant addition.

1. Introduction

Gas-liquid flow is recognized as the most complex two-phase flow, having many applications in petroleum, chemical and energy related industries (Bhagwat and Ghajar, 2016). Bubbly flow, which is characterized as a dispersion of gas bubbles in a continuous liquid phase, is encountered in numerous applications in oil and gas extraction plants, chemical/food/pharmaceutical industries, etc. (Colombo and Fairweather, 2016; Shen et al., 2015). Knowledge of bubbly flow characteristics is of great importance in designing multiphase systems, however, gaining full understanding of them is difficult due to the complex physics and multi-scale phenomena (Guan et al., 2015).

The majority of research studies examines the behaviour of bubbles in bubbly flows of Newtonian liquids. Nevertheless, most industrial processes, such as chemical and food engineering, polymer or glass manufacturing, fermentation and wastewater treatment, involve non-Newtonian liquids including polymers, slurries, emulsions, suspensions, etc. (Fu et al., 2011; 2015; Liu et al., 2013). Non-Newtonian liquids exhibit peculiar flow behaviour due to specific rheological properties, such as shear-thinning or shear-thickening, yield stress, viscoelastic characteristics, etc. Hence, bubbles rising in non-Newtonian liquids display complex behaviour much of which remains poorly understood (Amirnia et al., 2013; Li et al., 2012).

In addition, most studies focus on the formation and behaviour of single bubbles moving in Newtonian or non-Newtonian liquids (Böhm et al., 2014; Sun et al., 2015). Under certain conditions, however, bubbles can rise in gas-liquid flows as compact arrays, i.e. bubble clusters or swarms. Indicatively, Smolianski et al. (2008) numerically and Evgenidis and Karapantsios (2018) experimentally observed the presence of bubble clusters when studying bubble dynamics in viscous Newtonian liquids. Interestingly, both experimental and numerical studies indicate that the formation of clusters is particularly favoured during the motion of bubbles in non-Newtonian liquids (e.g. Vélez-Cordero et al., 2011; Vélez-Cordero and Zenit, 2011, 2014 and Zenit and Feng, 2018). Vélez-Cordero and Zenit (2011) showed that bubbles rising in non-Newtonian, shear-thinning liquids tend to form clusters of a certain size. These clusters differ from those formed in Newtonian liquids, regarding their density and compactness. In particular, the number of bubbles embedded in non-Newtonian (shear-thinning) clusters is higher than that found in Newtonian clusters. In addition, clusters appear to be more compact in shear-thinning liquids. Vélez-Cordero et al. (2011) and Zenit and Feng (2018) argued that clustering is triggered by a shear-thinning wake behind the bubbles. Bubbles rising in the low viscosity wake are less likely to disperse sideways into a high viscosity region. Once formed, bubble doublets or triplets ascend

* Corresponding author.
E-mail address: karapant@chem.auth.gr (T.D. Karapantsios).

https://doi.org/10.1016/j.ijmultiphaseflow.2020.103297
0301-9322/

Nomenclature

$\Delta t = t_2 - t_1$	duration of bubble cluster sensed by the electrical impedance spectroscopy technique
ε	volumetric void fraction
ε_1	void fraction value at the starting point of a signal peak
ε_2	void fraction value at the ending point of a signal peak
ε_{peak}	void fraction value at the maximum point of a signal peak
θ_{cone}	cone angle
μ_l	liquid dynamic viscosity
ρ_l	liquid density
σ_l	liquid surface tension
BSD	Bubble Size Distribution
CMC	carboxymethyl cellulose
D	internal pipe diameter
$D_{1,0}$	arithmetic average bubble diameter
DCS	Decompression Sickness
DKT	Drafting-Kissing-Tumbling
Eo	Eötvös number
g	gravity acceleration
Mo	Morton number
r_{cone}	cone radius
Re	Reynolds number as defined by Vélez-Cordero et al. (2011)
Re_l	liquid phase Reynolds number
SDS	Sodium Dodecyl Sulfate
t_1	time corresponding to ε_1
t_2	time corresponding to ε_2
t_{peak}	time corresponding to ε_{peak}
t_{total}	total electrical impedance signal (void fraction time-series) duration
U_{sg}	gas superficial velocity
U_{sl}	liquid superficial velocity
z/D	normalized axial distance

faster than single bubbles and capture more bubbles, resulting in the formation of a large bubble cluster that assumes an oblong shape and a nearly horizontal orientation. However, the aforementioned researchers stressed that a more shear-thinning liquid does not necessarily induce higher bubble clustering and concluded that Reynolds (*Re*) and Eötvös (Eo) numbers define the conditions for cluster formation: clustering is observed at small *Re* numbers (defined as $Re = \rho_l U_{sl} D_{1,0}/\mu_l$), i.e. when viscous forces are more important than inertial ones, and high Eo numbers (defined as $Eo = \rho_l g D^2_{1,0}/\sigma_l$), i.e. when gravitational forces are more important than surface tension forces. The tendency to form bubble clusters also increases with an increase of Morton (Mo) number (defined as $Mo = g\mu_l^4/\rho_l\sigma_l^3$) which is strictly dependant on liquid physical properties. The threshold of $Mo = 4 \times 10^{-4}$ was adopted by Vélez-Cordero and Zenit (2011) as the transition limit between 'clustering' and 'non-clustering' regimes, originally introduced by the numerical work of Smolianski et al. (2008). Furthermore, Vélez-Cordero et al. (2014) studied the terminal velocity of bubble clusters rising in Newtonian and non-Newtonian liquids and found that, although clusters behave as single bubbles, they do not experience the velocity jump discontinuity which is seen in single bubbles. Albeit some studies compare bubble clusters behaviour in Newtonian and non-Newtonian liquids, as well as the behaviour of bubble clusters and single bubbles, little is still known concerning the effect of operating conditions (U_{sg}, U_{sl}, etc.) or additives (surfactants, coagulation agents, etc.) on the behaviour of bubble clusters rising in non-Newtonian liquids.

This study is a follow up of the work of Gkotsis et al. (2019) who compared the effect of Newtonian and non-Newtonian blood-mimicking test liquids on void fraction and bubble size for the case of a gas-liquid flow resembling bubbly flow in human bloodstream during Decompression Sickness (void fraction values $< 10^{-1}$, bubble sizes < 1 mm). At relatively low U_{sl}, Gkotsis et al. (2019) noticed the presence of voluminous bubble clusters, consisting of sub-mm bubbles, when employing a non-Newtonian (shear-thinning) aqueous solution of glycerol, Xanthan gum and NaCl that resembles blood rheological behaviour under hyperviscosity syndrome conditions (e.g. ischaemic stroke, atherosclerosis, cyanotic congenital heart disease) (Broberg et al., 2006; Cho et al., 2014; Furukawa et al., 2016). The present study aims to associate for the first time the size and shape of such bubble clusters with features of electrical impedance signals acquired for void fraction estimation in gas-liquid flow. To do so, a superb void fraction measurement sensitivity is necessary. For this purpose, an EU patented electrical impedance spectroscopy technique of exceptionally high resolution is employed. Furthermore, this work examines the effect of gas superficial velocity (U_{sg}) and of surface tension on the behaviour of bubble clusters rising amongst single bubbles in a non-Newtonian, shear-thinning liquid. This work provides valuable information on bubble clustering encountered in ultrasound medical applications, such as dissolution of blood clots during thrombosis (histotripsy), cancer drug delivery, etc. (Lazarus et al., 2017; Maxwell et al., 2009).

2. Materials and methods

Experiments are conducted in a vertical, co-current, upward bubbly flow provided by a fully controllable flow loop (Fig. 1), which is capable of generating steady and pulsatile gas-liquid flow at various liquid/gas flow rates and bubble sizes. The present study concerns exclusively steady gas-liquid (bubbly) flow. Upward bubbly flow is examined inside a vertical tube 1.6 m long with internal diameter $D = 21$ mm, which is the typical diameter of human vena cava. Successive test sections of electrical, pressure, acoustical and optical diagnostics are placed along the vertical tube in order to determine void fraction and bubble features (size distribution and velocity). Here, only two diagnostics are exploited: a) an electrical impedance spectroscopy technique and b) an optical method. Liquid phase is recirculated through the flow loop by a progressive cavity pump (MD 025–6 L, Motovario S.p.A.) to supress cavitation in the liquid. Gas phase is injected through a cylindrical glass microporous filter (ROBU®; diameter: 10 mm, nominal pore size: 1.0–1.6 μm) which is located at the centre of the bottom of the vertical tube, where the two phases come in contact. The top filter wall is covered with glue to avoid large bubbles exiting and so the only bubbles allowed to enter the liquid flow are those generated and sheared-off at the side filter wall. Detailed information about the operation and specifications of experimental setup can be found in Evgenidis and Karapantsios (2015).

The EU patented, electrical impedance spectroscopy technique (Karapantsios et al., 2016) is used for the measurement of volumetric void fraction inside the vertical pipe. It employs innovative hardware and signal processing tools to capture void fraction fluctuations down to 10^{-5}. Such a measurement sensitivity, about two orders of magnitude higher compared to conventional electrical techniques, is important in this study. Electrical impedance measurements are conducted by a pair of metallic ring electrodes which are flush-mounted to the inner walls of the test tube at an axial distance of 59 cm ($z/D = 28$) from the gas injection point. The separation distance of electrodes is D/4, while the electrode width is D/10. Bubbly flow between the electrodes is electrically

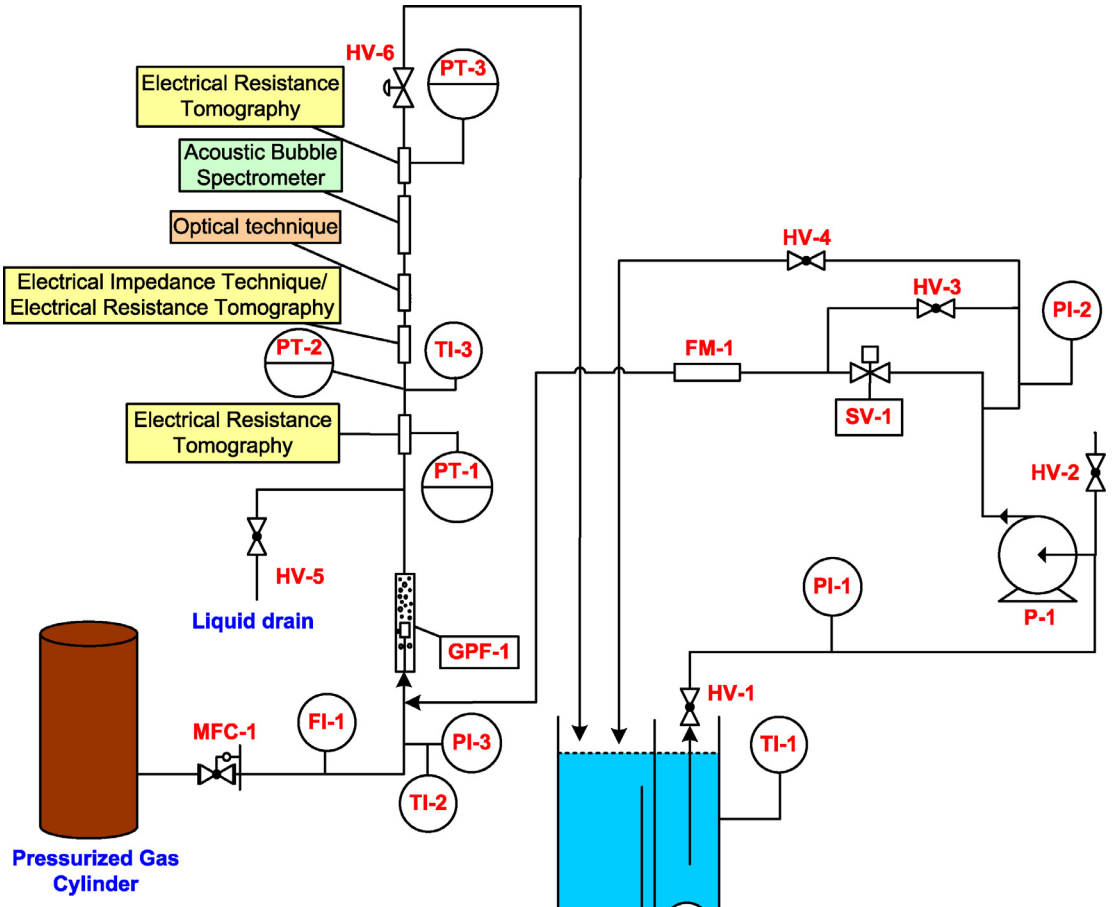

Code	Description
T-1	Liquid Tank
P-1	Progressive Cavity Pump
SV-1	Proportional Electromagnetic Valve
HC-1	Heater/Circulator
FM-1	Liquid Flow Meter
MFC-1	Gas Mass Flow Controller
FI-1	Gas Flow Meter
GPF-1	Glass Porous Filter
HV-1,2,3,4,5	On/Off Hand Valves
HV-6	Screw Down Hand Valve
TI-1,2,3	Temperature Indicators
PI-1,2,3	Pressure Indicators
PT-1,3	Differential Pressure Transducers
PT-2	Absolute Pressure Transducer

Fig. 1. Schematic layout of the experimental setup.

excited applying a sinusoidal voltage signal with an amplitude of $2V_{p\text{-}p}$. The frequency of the excitation signal is determined after a frequency sweep in the range 10–100 kHz looking for a value where electrodes polarization and capacitance contribution are supressed. The identified most appropriate excitation frequency is 25 kHz. All electrical signals are recorded by a high-resolution 24 bit data acquisition card (E-MU 1616 m, CREATIVE Professional) with a sampling frequency of 192 kHz. A custom Matlab routine is used for digitally processing and filtering the acquired signals. The final output of data reduction is a set of 60 s long electrical impedance time-series which are transformed to void fraction time-series through Maxwell model (Maxwell, 1892). More details about the operation of electrical impedance spectroscopy technique are found in Evgenidis and Karapantsios (2015).

Electrical measurements are performed simultaneously with optical ones using a method described in detail in Evgenidis and Karapantsios (2018). Bubbly flow images are captured at an axial distance of 75 cm ($z/D = 36$) above the gas injection point, employing CANON EOS 350D still digital camera equipped with proper macro lens (CANON EF 100 mm, f/2.8 Macro USM) and extension rings (CANON, 13–21–31 mm). Contrary to the study of Evgenidis and Karapantsios (2018) where bubbly flow images were processed to estimate bubble size distribution at different radial positions inside the vertical tube, optical measurements are exploited here only for a macroscopic characterization of bubble clusters (size and shape).

The employed test liquid is a shear-thinning aqueous solution which consists of glycerol (35% v/v, purity > 99%, Chem Lab),

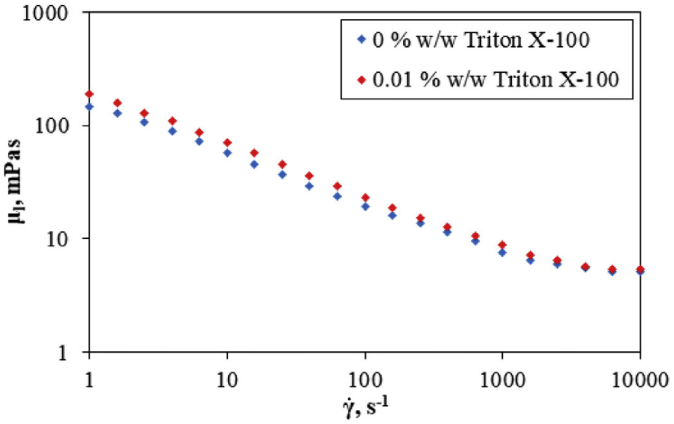

Fig. 2. Test liquid viscosity curves for 0% w/w and 0.01% w/w Triton X-100 at 37 °C.

NaCl (0.9% w/v, purity > 99.8%, Chem Lab) and Xanthan gum (1000 ppm, purity > 99.9%, Sigma-Aldrich) that simulates blood rheological behaviour under hyperviscosity syndrome conditions. Liquid superficial velocity, U_{sl}, remains constant during the experiments (2.89 cm/s), since bubble clustering is hindered at higher U_{sl} due to stronger flow inertia. Gas superficial velocity effect on the behaviour of bubble clusters is investigated employing three U_{sg} values (0.048, 0.217 and 0.385 cm/s). Furthermore, the influence of surface tension is examined by adding 0.01% w/w (100 ppm) Triton X-100 (purity > 99%, Sigma-Aldrich). Triton X-100 is a non-ionic surfactant, with Critical Micelle Concentration (CMC) around 189 ppm (Álvarez et al., 2015), which is employed routinely in gas-liquid flow applications in order to alter/adjust liquid surface tension with minimum effect on the ionic strength of the liquid. Electrical conductivity and pH of the examined liquids are measured with a pH–O_2-μS multimeter (ECM Multi, Dr. Lange), while surface tension is measured by a Wilhelmy plate tensiometer (TE2, Lauda Gmbh). Viscosity curves are obtained employing Physica MCR301 (Anton Paar) rheometer combined with a cone-plate system (r_{cone} = 2.5 cm, θ_{cone} = 1°) (Fig. 2). As shown in Fig. 2, both solutions exhibit shear-thinning behaviour due to Xanthan gum presence. A typical approximate formulation for the apparent viscosity, μ_l, of shear-thinning liquids is based on the power law model:

$$\mu_l = K * g^{(n-1)} \quad (1)$$

where K is the flow consistency index (i.e. the liquid viscosity at $\gamma = 1\ s^{-1}$), γ is the shear rate and n is the flow behaviour index. By fitting Eq. (1) to the viscosity curves of Fig. 2, the values of the above parameters are: K = 138.31 and n = 0.60 for the test liquid in the absence of Triton X-100, and K = 179.82 and n = 0.58 for the test liquid in the presence of 0.01% w/w Triton X-100, while the coefficient of determination R^2 is 0.986 and 0.990, respectively. Measured physical properties of test liquids at the temperature of 37 °C, where the experiments are conducted, are given in Table 1. Liquid phase Reynolds number (Re_l), defined as $Re_l = \rho_l U_{sl} D/\mu_l$, is almost 10 for the applied U_{sl} (2.89 cm/s) and, thus, the flow can be safely characterized as laminar. Helium gas (purity 99.9996%, Air Liquide) is chosen for bubbles production due to its low solubility in the test liquids.

3. Results and discussion

3.1. Bubble cluster formation

The formation of stable bubble clusters consisting of sub-mm bubbles in the gas-liquid flow of the present shear-thinning test liquid can be explained by a modified Drafting-Kissing-Tumbling (DKT) process. The DKT process has been originally proposed to describe bubble clustering for bubbles ranging from 1.5 mm to 4.5 mm (e.g. Vélez-Cordero et al., 2011 and Zenit and Feng, 2018). Yet its basic principle is still valid if somebody aims to explain clustering of sub-mm bubbles. During the first stage of the DKT process, a trailing bubble can easily approach a leading one due to viscosity gradients that appear in the wake of bubbles rising in a shear-thinning liquid and which reduce the repulsive force from bubble vortices (drafting stage). As a result a trailing bubble eventually touches the leading one (kissing stage). The third stage (tumbling) is not favourable in sub-mm bubbles. Such small bubbles behave like rigid spheres and cannot elongate or tumble across each other. Once two bubbles form a pair, they create a wake with lower viscosity which attracts more bubbles, leading to the formation of bubble clusters; however, the increase of cluster size decreases the viscosity gradient (so-attaining a Newtonian-like behaviour) and the growth of clusters then stops (Vélez-Cordero et al., 2011).

Vélez-Cordero and Zenit (2011) confirmed the threshold of Mo= 4×10^{-4}, that was first proposed by the numerical study of Smolianski et al. (2008), for the transition limit between 'clustering' and 'non-clustering' regimes when single bubble sizes range from 1.5 mm to 4.5 mm. Although single bubbles are much smaller in the present study (0.05 mm - 0.80 mm), bubble clusters are still observed when approximately Mo≥ 4×10^{-4} (Mo= 3.4×10^{-4} and 6.1×10^{-3}, in the absence and presence of Triton X-100, respectively). Addition of Triton X-100 strongly affects Mo, however, this is not crucial for bubble clustering since clusters are noticed even in the absence of surfactant. On the contrary, the presence of Xanthan gum is decisive for bubble clustering. First, it renders the test liquid non-Newtonian and, second, it increases liquid viscosity (lowering *Re* number). Both effects favour the formation of bubble clusters according to Vélez-Cordero et al., 2011 and Zenit and Feng (2018).

3.2. Influence of surface tension and gas superficial velocity on experimental data

This section investigates the effect of surface tension (by adding Triton X-100) and gas superficial velocity (U_{sg}) on experimental "raw" data, namely, void fraction time-series and bubbly flow images. Since glycerol, NaCl and Xanthan gum concentrations are

Table 1
Measured physical properties of the employed test liquids at 37 °C.

S/N	Test liquid composition			Test liquid physical properties		
	Glycerol (% v/v) / NaCl (% w/v) / Xanthan gum (ppm)	Triton X-100 (% w/w)	Surface tension (mN/m) (± 0.20)[a]	Density (kg/m^3) (± 1)[a]	Electrical conductivity (mS/cm) (± 0.01)[a]	Dynamic viscosity (mPas)[b] (± 0.05)[a]
1	35 / 0.9 / 1000	0	64.4	1109	6.85	5.18
2	35 / 0.9 / 1000	0.01	33.5	1108	6.85	5.34

[a] Refers to the average value of all runs.
[b] Value of the infinite-shear rate viscosity.

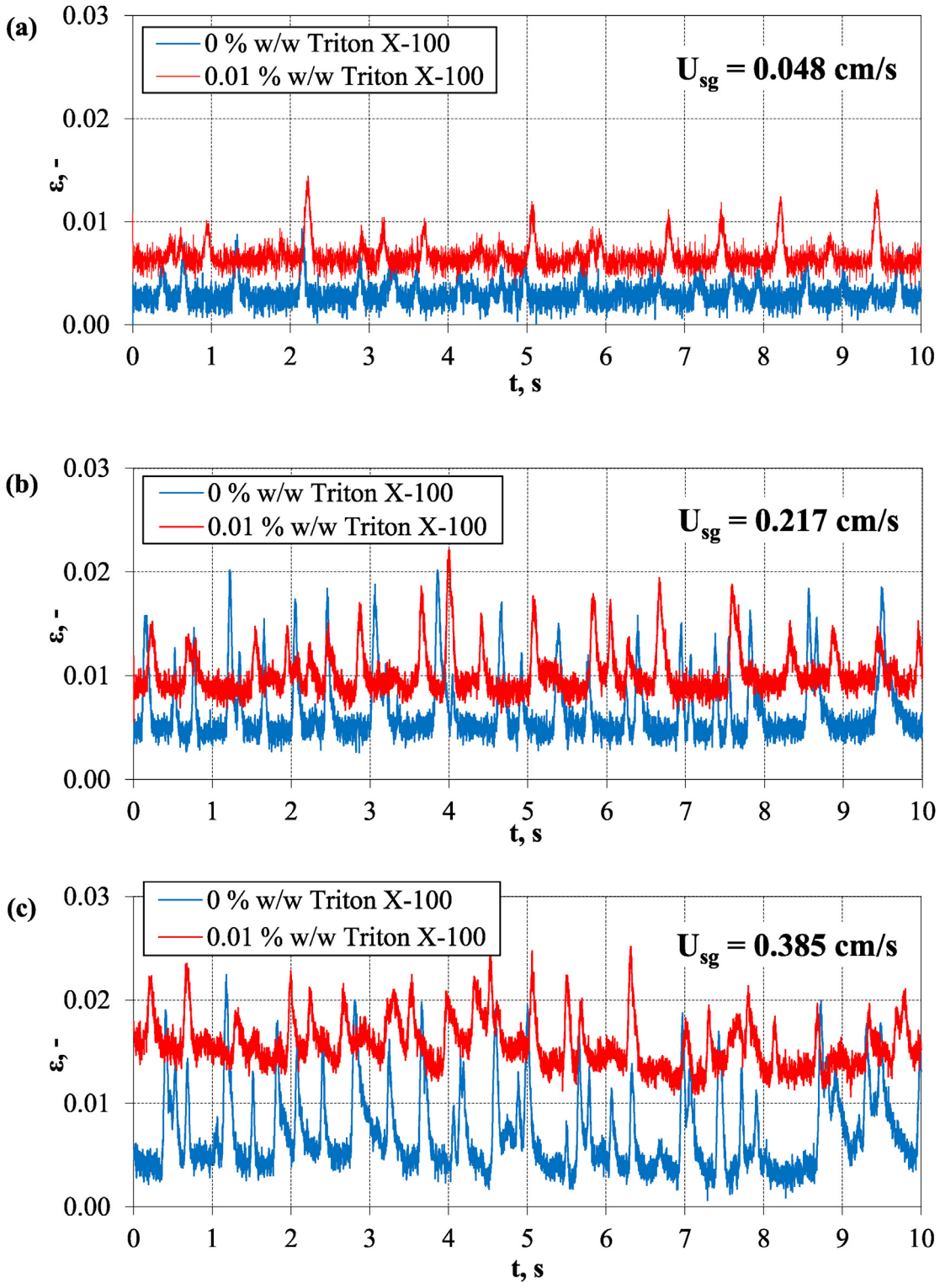

Fig. 3. Effect of Triton X-100 concentration on void fraction time series for: (a) U_{sg}= 0.048 cm/s, (b) U_{sg}= 0.217 cm/s and (c) U_{sg}= 0.385 cm/s.

constant in the examined test liquids, only Triton X-100 concentration is mentioned in the following figures.

3.2.1. Void fraction signals

Fig. 3 presents void fraction signals as a function of time in the absence and presence of Triton X-100 (0 and 0.01% w/w) and for three U_{sg} values (0.048, 0.217 and 0.385 cm/s). Although the acquired void fraction signals last 60 s, Figs. 3a, 3b and 3c display void fraction only for 10 s in an effort to discern typical signal features such as the intensity and frequency of observed peaks. The increase of U_{sg} and the presence of Triton X-100 both increase the instantaneous void fraction values. This has already been discussed by Gkotsis et al. (2019) over a broad range of U_{sl} values. The present study focuses on the investigation of void fraction signal peaks. These intense peaks are observed for all U_{sg} values and Triton X-100 concentrations and reflect the presence of bubble clus-

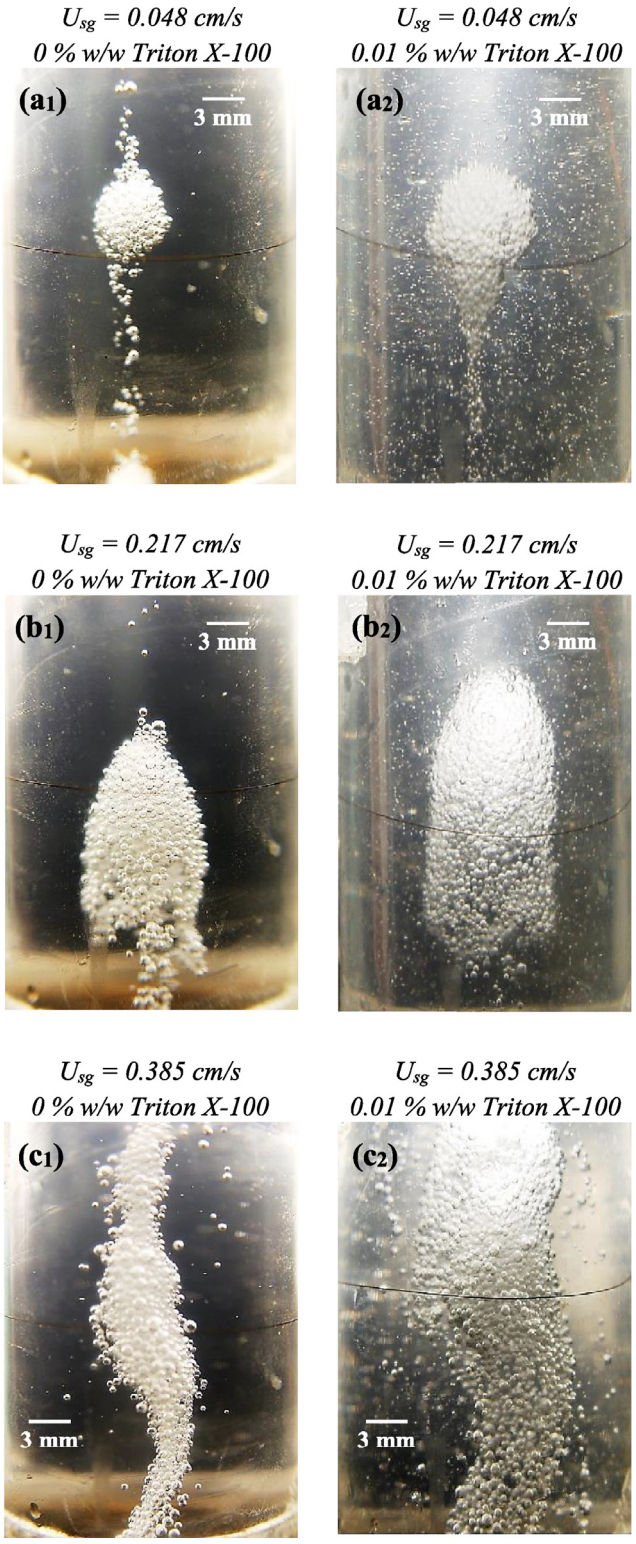

Fig. 4. Effect of gas superficial velocity (U_{sg}) on bubble clusters in the absence of Triton X-100 (a_1, b_1 and c_1) and in the presence of 0.01% w/w Triton X-100 (a_2, b_2 and c_2).

ters. It appears that the addition of Triton X-100 does not influence substantially the frequency of signal peaks. Contrarily, the intensity of signal peaks, seen as the difference from the baseline value, is affected considerably by the presence of surfactant, this being more evident at the medium and high U_{sg} values (0.217 and 0.385 cm/s, respectively).

On the other hand, increase of U_{sg} augments the frequency of signal peaks both in the presence and in the absence of Triton X-100. As regards the intensity of signal peaks, it increases from the low to the medium U_{sg} value but for a further increase to the highest U_{sg} value the intensity remains alike. There are two more interesting features in signal peaks as U_{sg} increases. First, peaks occupy longer time interval which means that as U_{sg} increases the baseline signal between peaks gets shorter and more disturbed. Second, peaks often appear as composite structures of two partially overlapping smaller peaks. The study of signal peaks' geometrical features as well as their correlation with the size and shape of bubble clusters is presented and discussed in Section 3.3.

3.2.2. Bubbly flow images

Fig. 4 displays representative bubbly flow images demonstrating the effect of gas superficial velocity (U_{sg}) and of the addition of Triton X-100 on the size and shape of bubble clusters. It is apparent that both properties are considerably influenced by U_{sg}. At the lowest U_{sg} (0.048 cm/s), bubble clusters are small and quite spherical (Figs. 4a_1 and 4a_2). Apart from isolated spherical clusters, batches of multiple clusters are also observed at this U_{sg} (see Supplementary Video 1 and Video 2). As U_{sg} increases (0.217 cm/s), clusters get larger in volume due to higher bubble collision frequency and become 'bullet-shaped' (Figs. 4b_1 and 4b_2). At the highest U_{sg} (0.385 cm/s), clusters become even larger and embrace an elongated, spiral shape which is quite different from the previous ones (Figs. 4c_1 and 4c_2). Similar chains of bubbles have been also reported previously in literature (Vélez-Cordero and Zenit, 2011; Vélez-Cordero et al., 2012, 2014). Interestingly, a dependence of bubble shape on bubble size has been registered even for single bubbles rising in non-Newtonian liquids. Amirnia et al. (2013) investigated upward bubbly flow in non-Newtonian solutions of Xanthan gum and carboxymethyl cellulose (CMC) and observed that bubble shape and motion gradually changed with the increase of bubble size: small bubbles were spherical and ascended strictly vertically, while larger bubbles had an ellipsoid shape and followed a spiral, 'zig-zag' course.

Although in our study each U_{sg} seems to favour the formation of a predominant cluster shape, different types of clusters are occasionally observed at a given U_{sg} value. Specifically, spherical clusters can be also noticed at higher U_{sg} values (0.217 cm/s and 0.385 cm/s), yet their number is limited. Similarly, a few 'bullet-shaped' clusters can be found at the highest U_{sg} value (0.385 cm/s). In contrast, elongated, spiral clusters are never observed at lower U_{sg} values (0.048 and 0.217 cm/s). Furthermore, bubble clusters are dynamic in structure as they rise amongst other ascending indi-

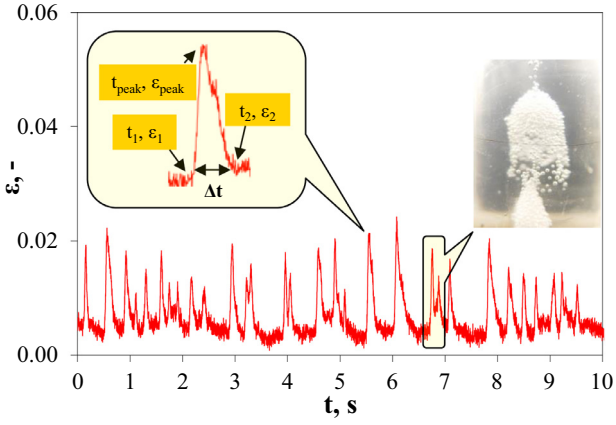

Fig. 5. Definition of parameters of void fraction signal peaks caused by the presence of bubble clusters.

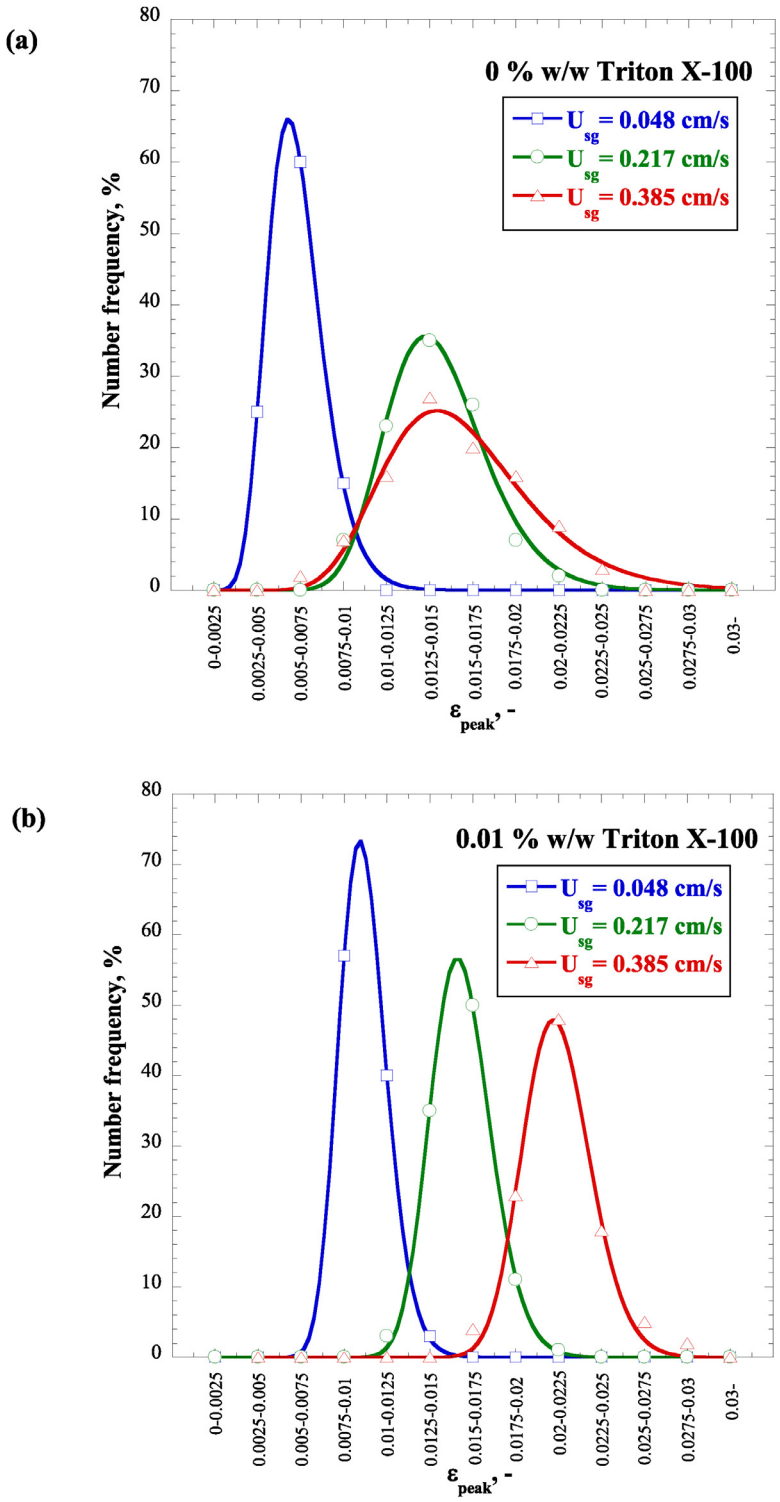

Fig. 6. Effect of gas superficial velocity (U_{sg}) on ε_{peak} distribution: (a) in the absence of Triton X-100 and (b) in the presence of Triton X-100 (0.01% w/w).

vidual bubbles, depending on the U_{sg} value. At U_{sg}= 0.048 cm/s, nearly spherical clusters are relatively unstable and tend to break into smaller clusters. At U_{sg}= 0.217 cm/s, 'bullet-shaped' clusters are disrupted less frequently, while disruption of clusters is very limited at the highest U_{sg} value (0.385 cm/s).

The effect of Triton X-100 addition on the properties of bubble clusters is less intense. The comparison of Figs. 4a_1, 4b_1 and 4c_1 with Figs. 4a_2, 4b_2 and 4c_2, respectively, shows that the decrease of liquid surface tension due to surfactant addition increases by a small extent the size of the clusters (in both diameter and length) and has little effect on their shape. Gkotsis et al. (2019) showed that this concentration of surfactant leads to about 30% smaller diameter of bubbles. Due to their small size these bubbles are more rigid (immobile interface) and less affected by buoyancy. Another clear consequence of the addition of surfactant is the co-existence of a large number of single bubbles together with bubble clusters. The above may explain, at least partially, the overall higher void fraction values in the presence of surfactant in Fig 3.

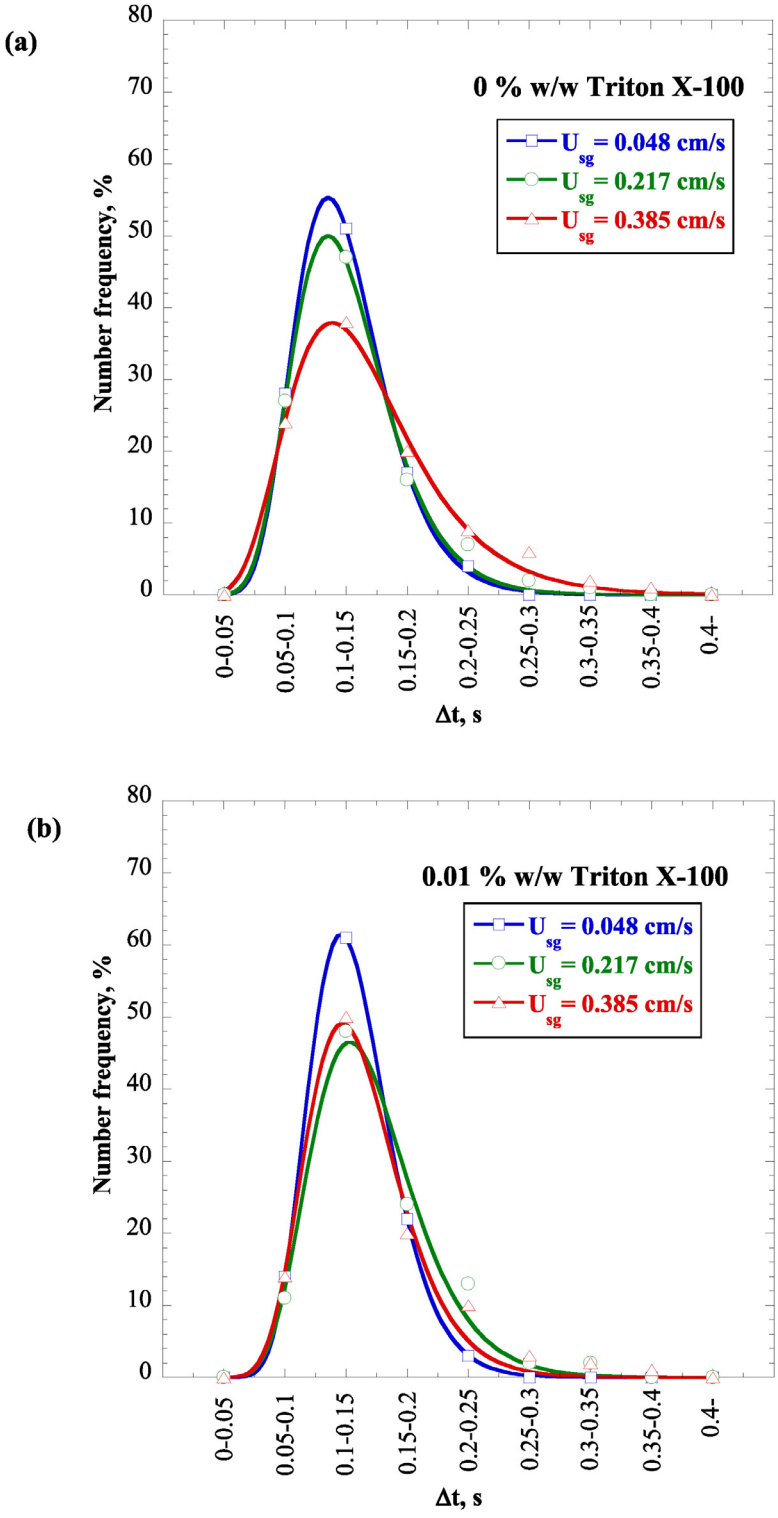

Fig. 7. Effect of gas superficial velocity (U_{sg}) on Δt distribution: (a) in the absence of Triton X-100 and (b) in the presence of Triton X-100 (0.01% w/w).

3.3. Analysis of void fraction signal peaks

In this section, an attempt is made to correlate the size and shape of bubble clusters with geometrical features of void fraction signal peaks caused by their presence. Fig. 5 displays a part of a typical void fraction time-series. In every peak three key parameters are identified: starting point, maximum point and ending point. Interestingly, several double peaks are sporadically noticed apart from single peaks which correspond to isolated bubble clusters. Careful examination of the obtained bubbly flow images demonstrated that these peaks are caused by the presence of consecutive bubble clusters rising inside the vertical pipe. As shown in Fig. 5, the following peak parameters are determined in all electrical impedance signals (void fraction time-series) of 60 s:

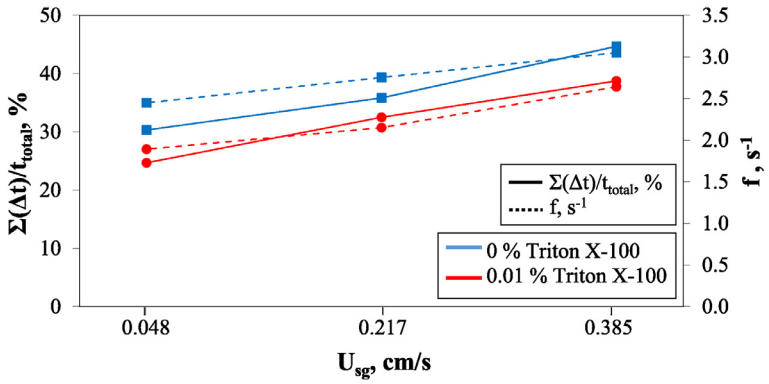

Fig. 8. Effect of gas superficial velocity (U_{sg}) and Triton X-100 concentration on% duration of bubble clusters presence in the void fraction (electrical) signal ($\Sigma(\Delta t)/t_{total}$) and frequency of bubble clusters (f).

- ε_{peak}: void fraction value at the maximum point of each peak,
- ε_1: void fraction value at the starting point of each peak,
- ε_2: void fraction value at the ending point of each peak,
- t_{peak}: time corresponding to ε_{peak},
- t_1: time corresponding to ε_1,
- t_2: time corresponding to ε_2,
- $\Delta t = t_2 - t_1$: duration of bubble cluster sensed by the electrical impedance spectroscopy technique.

It is understood that ε_{peak} and Δt are the key peak parameters to be correlated with the size and shape of bubble clusters. Since cluster properties depend on U_{sg} and surface tension, the effect of these parameters on the aforementioned quantities is examined in detail.

Fig. 6 shows the effect of U_{sg} and Triton X-100 addition on the distribution of ε_{peak} values measured in the void fraction time-series. It is seen that ε_{peak} distribution shifts to higher values with the increase of U_{sg}, both in the absence and in the presence of Triton X-100 (0.01% w/w). This may be attributed to a higher overall void fraction in the flow as U_{sg} increases. This has been clearly observed in Fig. 3. However, optical measurements indicate that cluster sizes increase, too, with U_{sg} and larger clusters also cause higher ε_{peak} values. In the absence of surfactant, successive clusters are observed to be well separated from each other in the axial (flow) direction, so the measured electrical signal clearly alternates between a minimum baseline value, when only dispersed single bubbles pass by the measuring volume of the impedance technique, and a maximum peak value, when a cluster passes by. However, in the presence of surfactant, clusters are larger and longer and separation between successive clusters is not so definite. So, at every instant there is part of a cluster inside the measuring volume and this yields an increased void fraction baseline and smaller $\varepsilon_{peak}-\varepsilon_{base}$ values. On this account, the statistics of ε_{peak} are more representative than the statistics of $\varepsilon_{peak}-\varepsilon_{base}$ because the latter are biased by the increased baseline value due to the finite size of the measuring volume. This is in line with optical observations.

The width of ε_{peak} distribution increases with U_{sg} indicating the presence of different clusters in size and shape, as already discussed in Section 3.2.2. From a quantitative point of view, this effect is more intense in the absence of surfactant. Regarding the effect of liquid surface tension, the decrease caused by Triton X-100 addition increases ε_{peak} for all U_{sg} values. The presence of surfactant on bubbles surface creates a surface elasticity that renders the surface practically immobile. Consequently, bubbles: a) rise with lower velocity, b) approach each other more easily and c) form clusters which are larger in size, resulting in the shift of ε_{peak} to higher values.

Fig. 7 presents the effect of U_{sg} and Triton X-100 addition on Δt distribution of each electrical impedance signal. This quantity is meaningful despite the biased baseline due to the finite measuring volume. This is so because signal peaks are steep and so errors associated with the position of the starting and ending points of peaks are small. As already discussed, bubble clusters become larger and longer with U_{sg}. At first glance, one would expect a notable increase of Δt, which corresponds to the duration of bubble clusters sensed by the electrical impedance technique. However, Fig. 7 shows only a slight shift of Δt distribution to higher values with an increase of U_{sg}, both in the absence and in the presence of Triton X-100. This might be explained by considering that larger clusters experience higher buoyant velocities. In other words, as clusters get larger they rise faster and so Δt remains almost constant. For the same reason, Δt is not influenced by the addition of Triton X-100, as well.

The ratio $\Sigma(\Delta t)/t_{total}$ (%) and the frequency of bubble clusters (f, s^{-1}) are two important statistical quantities that can be calculated for each electrical impedance signal. Ratio $\Sigma(\Delta t)/t_{total}$ is the sum of all peaks duration in a time series divided by the total time series duration (t_{total}) and expresses the% duration of bubble clusters presence in the signal. However, this ratio cannot provide valuable information about the number of bubble clusters, since a specific value of $\Sigma(\Delta t)/t_{total}$ may result either from a few large clusters, or from many smaller ones. For this purpose, frequency of bubble clusters presence is determined separately. It is defined as the number of bubble clusters (ε_{peak}) detected by the electrical impedance technique per time unit.

Fig. 8 presents the effect of U_{sg} and Triton X-100 addition on the ratio $\Sigma(\Delta t)/t_{total}$ and the frequency of bubble clusters (f). It is shown that both statistical quantities increase with U_{sg}. This means that more bubble clusters are formed per unit time and their contribution in void fraction signals (by means of signal spikes) becomes more intense. On the other hand, Triton X-100 addition lowers the liquid surface tension and decreases the frequency of bubble clusters. As mentioned above, surfactant addition causes a small increase of cluster sizes. Apparently, for a given U_{sg} value, an increase of cluster sizes implies the formation of less clusters. Interestingly, the decrease of bubble clusters' number dominates over the increase of their size, resulting in the decrease of the ratio $\Sigma(\Delta t)/t_{total}$ as well.

4. Conclusions

This work examines the behaviour of bubble clusters rising along with single bubbles in a shear-thinning blood-mimicking liquid which consists of glycerol, NaCl and Xanthan gum. Bubble clusters are experimentally investigated by means of an electrical

impedance spectroscopy technique for void fraction determination and an optical method for the estimation of their size and shape. Clustering is strongly favoured by Xanthan gum presence that renders test liquid non-Newtonian and increases liquid viscosity. Although bubble clusters consist of sub-mm bubbles, their formation is noticed when $Mo \geq 4 \times 10^{-4}$, a threshold value suggested in literature for larger bubbles (1.5 mm - 4.5 mm). The size and shape of clusters are significantly influenced by gas superficial velocity: clusters are small and quite spherical at U_{sg}= 0.048 cm/s, larger and 'bullet-shaped' at U_{sg}= 0.217 cm/s and even larger and elongated/spiral at U_{sg}= 0.385 cm/s. On the contrary, a decrease of liquid surface tension (by adding Triton X-100) increases slightly the size of clusters and has little effect on their shape.

Bubble clusters cause intense peaks on acquired void fraction (electrical) signals. These peaks are observed for all U_{sg} values and Triton X-100 concentrations and their features (ε_{peak}: void fraction value at the maximum point of each peak, Δt: duration of bubble cluster) can be associated with cluster size and shape. Specifically, ε_{peak} distribution shifts to higher values with increasing U_{sg} and decreasing liquid surface tension that make clusters larger. On the other hand, Δt remains almost constant with increasing U_{sg} and decreasing surface tension. This has been attributed to the higher cluster buoyant velocity as cluster size increases. The ratio $\Sigma(\Delta t)/t_{total}$ (%)and the frequency of bubble clusters (f, s^{-1}) are two key statistical quantities calculated for each electrical impedance signal. Results demonstrate that both of them increase with U_{sg} and decrease with Triton X-100 addition.

Declaration of Competing Interest

The authors declare that they have no known competing financial interests or personal relationships that could have appeared to influence the work reported in this paper.

CRediT authorship contribution statement

Petros K. Gkotsis: Methodology, Investigation, Formal analysis, Writing - original draft, Visualization. **Sotiris P. Evgenidis:** Conceptualization, Methodology, Validation, Writing - review & editing, Funding acquisition. **Thodoris D. Karapantsios:** Validation, Resources, Writing - review & editing, Supervision, Project administration.

Acknowledgements

This research is co-financed by Greece and the European Union (European Social Fund- ESF) through the Operational Programme «Human Resources Development, Education and Lifelong Learning» in the context of the project "Reinforcement of Postdoctoral Researchers" (MIS-5001552), implemented by the Greek State Scholarships Foundation (ΙΚΥ).

References

Álvarez, M.S., Patiño, F., Deive, F.J., Sanromán, M.A., Rodríguez, A., 2015. Aqueous immiscibility of cholinium chloride ionic liquid and Triton surfactants. J. Chem. Thermodynamics 91, 86–93.
Amirnia, S., De Bruyn, J.R., Bergougnou, M.A., Margaritis, A., 2013. Continuous rise velocity of air bubbles in non-Newtonian biopolymer solutions. Chem. Eng. Sci. 94, 60–68.
Bhagwat, S.M., Ghajar, A.J., 2016. Experimental investigation of non-boiling gas-liquid two phase flow in upward inclined pipes. Exp. Therm. Fluid Sci. 79, 301–308.
Böhm, L., Kurita, T., Kimura, K., Kraume, M., 2014. Rising behaviour of single bubbles in narrow rectangular channels in Newtonian and non-Newtonian liquids. Int. J. Multiph. Flow 65, 11–23.
Broberg, C.S., Bax, B.E., Okonko, D.O., Rampling, M.W., Bayne, S., Harries, C., Davidson, S.J., Uebing, A., Khan, A.A., Thein, S., Gibbs, J.S.R., Burman, J., Gatzoulis, M.A., 2006. Blood Viscosity and its Relationship to Iron Deficiency, Symptoms, and Exercise Capacity in Adults With Cyanotic Congenital Heart Disease. J. Am. Coll. Cardiol. 48 (2), 356–365.
Cho, Y.I., Cho, D.J., Rosenson, R.S., 2014. Endothelial Shear Stress and Blood Viscosity in Peripheral Arterial Disease. Curr. Atheroscel. Rep. 16 (404), 1–10.
Colombo, M., Fairweather, M., 2016. RANS simulation of bubble coalescence and break-up in bubbly two-phase flows. Chem. Eng. Sci. 146, 207–225.
Evgenidis, S.P., Karapantsios, T.D., 2015. Effect of bubble size on void fraction fluctuations in dispersed bubble flows. Int. J. Multiph. Flow 75, 163–173.
Evgenidis, S.P., Karapantsios, T.D., 2018. Gas-liquid flow of sub-millimeter bubbles at low void fractions: experimental study of bubble size distribution and void fraction. Int. J. Heat Fluid Fl. 71, 353–365 2018.
Fu, T., Ma, Y., Funfschilling, D., Li, H.Z., 2011. Bubble formation in non-Newtonian fluids in a microfluidic T-junction. Chem. Eng. Process. 50, 438–442.
Fu, T., Ma, Y., Li, H.Z., 2015. Flow patterns of liquid-liquid two-phase flow in non-Newtonian fluids in rectangular microchannels. Chem. Eng. Process. 91, 114–120.
Furukawa, K., Abumiya, T., Sakai, K., Hirano, M., Osanai, T., Shichinohe, H., Nakayama, N., Kazumata, K., Hida, K., Houkin, K., 2016. Increased Blood Viscosity in Ischemic Stroke Patients with Small Artery Occlusion Measured by an Electromagnetic Spinning Sphere Viscometer. J. Stroke Cerebrovasc. Dis. 25 (11), 2762–2769.
Gkotsis, P.K., Evgenidis, S.P., Karapantsios, T., 2019. Influence of Newtonian and non-Newtonian fluid behaviour on void fraction and bubble size for a gas-liquid flow of sub-millimeter bubbles at low void fractions. Exp. Therm. Fluid Sci. 109, 109912.
Guan, X., Li, Z., Wang, L., Li, X., Cheng, Y., 2015. A dual-scale turbulence model for gas-liquid bubbly flows. Chin. J. Chem. Eng. 23, 1737–1745.
Karapantsios, T.D., Evgenidis, S.P., Zacharias, K., Mesimeris, T., 2016. Method for the detection and characterization of bubbles in liquids and device therefor, resp. system. European Patent Office 3005942, A1.
Lazarus, C., Pouliopoulos, A.N., Tinguely, M., Garbin, V., Choi, J.J., 2017. Clustering dynamics of microbubbles exposed to low-pressure 1-MHz ultrasound. J. Acoust. Soc. Am. 142, 3135–3146.
Li, S., Ma, Y., Zhu, C., Fu, T., Li, H., 2012. Turbulent Characteristic of Liquid Around a Chain of Bubbles in Non-Newtonian Fluid. Chin. Journal of Chem. Eng. 20, 883–888.
Liu, J., Zhu, C., Fu, T., Ma, Y., Li, H., 2013. Numerical simulation of the interactions between three equal-interval parallel bubbles rising in non-Newtonian fluids. Chem. Eng. Sci. 93, 55–66.
Maxwell, A.D., Cain, C.A., Duryea, A.P., Yuan, L., Gurm, H.S., Xu, Z., 2009. Non-Invasive Thrombolysis Using Pulsed Ultrasound Cavitation Therapy - Histotripsy. Ultrasound Med Biol 35 (12), 1982–1994.
Maxwell, J.C., 1892. A Treatise of Electricity and Magnetism. Oxford University Press, London.
Shen, X., Hibiki, T., Nakamura, H., 2015. Bubbly-to-cap bubbly flow transition in a long-26 m vertical large diameter pipe at low liquid flow rate. Int. J. Heat Fluid Flow 52, 140–155.

Ευρωπαϊκή Ένωση
European Social Fund

Operational Programme
Human Resources Development,
Education and Lifelong Learning
Co-financed by Greece and the European Union

ΕΣΠΑ 2014-2020
ανάπτυξη - εργασία - αλληλεγγύη

Smolianski, A., Haario, H., Luukka, P., 2008. Numerical study of dynamics of single bubbles and bubble swarms. Appl. Math. Model. 32, 641–659.
Sun, B., Guo, Y., Wang, Z., Yang, X., Gong, P., Wang, J., Wang, N., 2015. Experimental study on the drag coefficient of single bubbles rising in static non-Newtonian fluids in wellbore. J. Nat. Gas Sci. Eng. 26, 867–872.
Vélez-Cordero, J.R., Lantenet, J., Hernández-Cordero, J., Zenit, R., 2014. Compact bubble clusters in Newtonian and non-Newtonian liquids. Phys. Fluids 26, 053101.
Vélez-Cordero, J.R., Sámano, D., Yue, P., Feng, J.J., Zenit, R., 2011. Hydrodynamic interaction between a pair of bubbles ascending in shear-thinning inelastic fluids. J. Non-Newton. Fluid Mech. 166, 118–132.
Vélez-Cordero, J.R., Sámano, D., Zenit, R., 2012. Study of the properties of bubbly flows in Boger-type fluids. J. Non-Newton. Fluid Mech 175-76, 1–9.
Vélez-Cordero, J.R., Zenit, R., 2011. Bubble cluster formation in shear-thinning inelastic bubbly columns, J. Non-Newton. Fluid Mech. 166, 32–41.
Zenit, R., Feng, J.J., 2018. Hydrodynamic interactions among bubbles, drops, and particles in non-Newtonian liquids. Annu. Rev. Fluid. Mech 50, 505–534.